Praca oryginalna *Original paper*

Antioxidant and anti-inflammatory effects of cerium oxide *Salvia veneris* nanoparticles on acetamiprid-induced renal and hepatic toxicity in rats

EMRAH CAYLAK

Department of Biochemistry, Post-Doc, Health Sciences Institute, Firat University, Elazig, Turkiye

Received 13.06.2024 *Accepted 16.07.2024*

Caylak E.

Antioxidant and anti-inflammatory effects of cerium oxide *Salvia veneris* nanoparticles on acetamiprid-induced renal and hepatic toxicity in rats

Summary

This study investigates the antioxidant/anti-inflammatory activities of *S. veneris* extract (SvE) and cerium oxide nanoparticles/*S. veneris* (CeO_2-NPs/SvE). The study first analyzed the total polyphenolic, flavonoid, and saponin contents of SvE. The identification of phenolic compounds was determined using High-Performance Liquid Chromatography (HPLC). Next, the study investigated the hepatoprotective and nephroprotective effects of *S. veneris* on acetamiprid-induced toxicity in rats. The rats were administered acetamiprid orally for two weeks, alone or in combination with SvE and CeO_2-NPs/SvE. Our study found an association between acetamiprid-induced toxicity and significant changes in biochemical, histopathological, antioxidant, and anti-inflammatory parameters. The treatment with SvE and CeO_2-NPs/SvE resulted in a reduction of malondialdehyde (MDA), TNF-α and IL-6 cytokine levels, while increasing glutathione (GSH) as superoxide dismutase (SOD) and glutathione peroxidase (GSH-Px), IL-10 and TGF-β levels. Our study suggests that cerium oxide nanoparticles synthesized from *S. veneris* using the green synthesis method could be a protective and therapeutic agent against various diseases.

Keywords: antioxidant, anti-inflammatory, *Salvia veneris*, acetamiprid, nephrotoxicity, hepatotoxicity

The *Salvia veneris* plant (sage), a type of sage, belongs to the Lamiaceae family. Sage has been used for various medicinal purposes, including as an analgesic, stomach soother, lung disinfectant, diuretic, and neuro-relaxant for respiratory diseases such as colds, flu, bronchitis, and asthma. It has also been used for rheumatism, heart diseases, skin infections, and women's diseases such as galactorrhoea and menopause. Additionally, it has been studied for its potential in treating various cancers. This medicinal plant, *Salvia* spp., has been found to contain polyphenols, phenolics, flavonoids, sterols, terpenoids, and essential oils (36). Its phenolic and flavonoid chemical compositions have been studied and have antioxidant, antibacterial, anti-inflammatory, antidiabetic, tumor suppressor, hepatoprotective, analgesic, antipyretic, and insecticidal properties. Although extracts from *Salvia* spp. have been extensively studied (13, 18, 36), *S. veneris* is an endemic plant of Cyprus that has not been previously studied *in vivo* for its antioxidant, anti-inflammatory, nephroprotective, and hepatoprotective properties. It is a pink-flowered perennial herb that grows in rocky areas with 1100-1950 m streams. It has been found in Degirmenlik village (Nicosia) and the sides of the mountain area between Taskent and Buffavento (Kyrenia) in North Cyprus (13).

Acetamiprid is a neonicotinoid insecticide used in agriculture to protect vegetables and fruits from insects. It is a significant risk factor due to its toxicity to human health and the environment. It binds to the acetylcholine receptors of the central nervous system in insects, interrupting synaptic transmission (25). Food contamination with insecticide residues from agricultural activities can lead to accumulation in the

kidney, liver, and thyroid gland tissues of humans and animals. This can result in nephrotoxic, hepatotoxic, neurotoxic, and immunotoxic effects, potentially leading to increased reactive oxygen species (ROS) and death. Subchronic exposure to acetamiprid results in a decrease in the activity of antioxidant enzymes, particularly liver antioxidant superoxide dismutase (SOD), catalase (CAT), and glutathione peroxidase (GPx) (25).

There is no comprehensive research on the phytochemical content of extracts obtained from *S. veneris*. The scientific community has been studying the production of metal nanoparticles from plant extracts using green biosynthesis and exploring the potential biomedical applications of CeO_2-NPs. Using nanoparticles in animal health and veterinary medicine will also benefit treating animal diseases. Combining radiographic imaging technologies with nanoparticles in experimental animal studies offers a less invasive alternative to traditional biopsy methods (16). Using cerium nanoparticles to encapsulate liposome drugs is promising for animal wound treatments (11). Titanium dioxide nanoparticles have also shown promising antioxidant and antimicrobial properties in animal heart diseases (29), and cerium nanoparticles in wound healing and diabetic foot ulcer treatment (3, 17). For instance, *in vivo*, results have shown that CeO_2-NPs have biological properties that can accelerate wound healing by promoting angiogenesis, reducing inflammation, and preventing infections (2, 24). CeO_2-NPs can also reduce the side effects of conventional antiviral drugs in the treatment and increase the concentration of metal nanoparticles or drug molecules in specific organs or tissues. In addition, targeted metal nanoparticles can prevent the spread of the virus and infections to vital organs. CeO_2-NPs have been proposed against COVID-19 because of their antiviral, antioxidant, and immunomodulatory properties (23). A few researchers have shown that CeO_2-NPs can suppress pro-inflammatory markers and oxidative stress against ischemic heart disease (34), steatohepatitis, and portal hypertension (12). Some researchers have also demonstrated that CeO_2-NPs can protect the morphology and viability of neuronal cells from injury through their antioxidant and signal transduction modulation activities in Alzheimer's disease (35).

The significant advantage of using nanoparticles produced through green biosynthesis is that they contain metal ions or functional groups that can reduce free radicals in their structures. When free oxygen radicals (FOR) are produced within cells due to metabolic disorders or cellular interactions with external substances, excess reactive oxygen-nitrogen species cause oxidative and nitrative stresses. These stresses damage cell membranes, proteins, and DNA, ultimately resulting in cell death. Cerium oxide nanoparticles (CeO_2-NPs) have large reactive surface areas within a fluorite crystalline lattice structure and can serve as catalysts and antioxidants. The transition from a reduced to an oxidized state emulates the properties of antioxidant enzymes such as SOD, catalase, and peroxidase to neutralize free radicals (9, 10).

Our study aimed to examine the antioxidant, anti-inflammatory, hepatoprotective, and nephroprotective effects of *S. veneris* plant extract (SvE) and the synthesized CeO_2-NPs of *S. veneris* (CeO_2-NPs/SvE) on acetamiprid-induced oxidative stress in rats.

Material and methods

Chemistry. During the flowering period, *S. veneris* plants were harvested from the mountainous area between Taskent and Buffavento (Kyrenia) in North Cyprus. The leaves and flowers were dried in the shade for two weeks and then powdered using an electric plant grinder. All chemicals and cerium nitrate [$Ce(NO_3)_3 \cdot 6H_2O$] used in the study were supplied by Merck Company (Germany).

Preparation of *S. veneris* extract. 100 g of dried *S. veneris* was placed in a volumetric flask, and 1500 ml of 100% methanol (Merck, Germany) was added for extraction. The mixture was continuously macerated at room temperature for 24 hours. The resulting extracts were centrifuged at 4000 rpm for 10 minutes and filtered using Whatman 1 filter paper. The mixture's solvent fraction underwent evaporation using a rotary evaporator (IKA RV 10 with HB 10 bath, Germany) and was subsequently redissolved in methanol. The resulting solution was stored in a refrigerator at 4°C until further analysis.

Phytochemical analysis of the *S. veneris* extract

Quantification of phenolic compounds. The polyphenolic content of *S. veneris* extract was determined using the Folin-Ciocalteu colorimetric method (28). In a test tube, 30 µl of SvE, 3 ml of Folin Ciocalteu reagent, and 3 ml of Na_2CO_3 were mixed and incubated at 20°C for 1 hour. The solution turned blue, and its absorbance was measured at 760 nm using a UV spectrophotometer (Shimadzu UV 1800, Japan). The reference chemical substance used was gallic acid, and the results are expressed as mg GA/g SvE.

The total flavonoid content of *Salvia veneris* extract was determined using the aluminum chloride colorimetric method (28). 60 µl of SvE, 4 ml of distilled water, and 20 µl of aluminium chloride reagent (10% methanol) were added to 10 ml volumetric bottles to prepare the sample. The volume was then completed to 5 ml with pure methanol. The mixture was incubated at 20°C for 30 minutes, and its absorbance was measured at 430 nm using a UV spectrophotometer. Quercetin was used as the reference chemical, and the values are expressed as mg quercetin/g *S. veneris* extract.

The total saponin content of SvE was determined using the acetic-sulfuric acid method (28). In a test tube containing 500 µl of SvE, 1000 µl of glacial acetic acid and 1000 µl of sulfuric acid were added and mixed thoroughly. The mixture was heated at 60°C for 30 minutes and then rapidly cooled to 20°C using an ice water bath. The solution turned purple, and its absorbance was measured at 530 nm using a UV spectrophotometer. Oleanolic acid was used as the reference chemical, and the values are expressed as mg oleanolic acid per gram of SvE.

HPLC analysis. Quantization and identification of phenolic compounds of SvE were performed using HPLC (Agilent 1200, CA, USA). The plant extracts were prepared beforehand and dissolved in 100 µg/ml of distilled water. After homogenization with a vortex, 20 µl of the extract was filtered and injected into the HPLC column. The programmed flow rate was 10 ml/min, with a temperature of 30°C and elution gradients of B linear 5-15%, 0-3 min; 15-25%, 4-13 min, 25-30%, 14-25 min; 30-40%, 26-35 min; 40-43%, 36-40 min; 43-47%, 41-50 min; 47-100%, 51-54 min. The mobile phase solvents were water/acetic acid (98/2, v/v) and methanol (28). The absorption spectra were measured in triplicate within the 280 nm to 400 nm range. The SvE phytochemicals were identified by comparing retention times and UV spectra with Agilent ChemStation software (Hewlett-Packard ChemStation System). The identified molecules include apigenin, caffeic acid, catechin, coumarin, coumaric acid, ferulic acid, gallic acid, kaempferol, luteolin, myricetin, rosmarinic acid, rutin, sinapic acid, syringic acid, tannic acid, trans-cinnamic acid, and vanillic acid. The values were expressed as µg/g SvE.

Synthesis and analysis of CeO_2 nanoparticles. CeO_2 nanoparticles of *S. veneris* (CeO_2-NPs/Sv) were synthesized using $[Ce(NO_3)_3 \cdot 6H_2O]$. 4.34 g of cerium nitrate was added to 100 ml of SvE in a beaker and mixed using a magnetic hotplate at 50°C. The mixture was vortexed at 1500 rpm for 2 hours, resulting in the formation of CeO_2-NPs/SvE, indicated by the blackish-brown color of the solution. The nanoparticles were then purified by centrifugation at 10,000 rpm for 10 minutes, and the yellow-colored nanoparticle pellets were collected and freeze-dried with Alpha 1-2 LD (–80°C). The maximum absorbance of CeO_2-NPs/SvE was determined using a UV spectrophotometer with a range of 300-400 nm. Structural and size analysis were conducted using Scanning Electron Microscopy (SEM) and Transmission Electron Microscopy (TEM) (Hitachi, Japan). X-ray diffraction (XRD) analysis was performed using an X'Pert Powder nickel monochromator (PANalytical, Holland) (2θ : 20°-80°, Cu/Kα radiation in 1.540 Å) to examine their crystallographic structure. The spectral properties of the sample were analyzed using Fourier Transform Infrared Spectroscopy (FTIR) (Shimadzu, Japan) in the range of 4000-400 cm^{-1} (24).

***In vivo* study**

Experimental design of animals. We obtained healthy male and adult Sprague-Dawley rats weighing 220 ± 30 g from a commercial source. Their health conditions are guaranteed by the commercial company and sold. The animals were fed standard mouse chow and given tap water. They were housed in autoclavable polycarbonate cages under standard environmental conditions, including a room temperature of 20°C, 50% humidity, and a 12-hour light/dark cycle. Ten rats were randomly assigned to each group. The substances were dissolved in olive oil and administered intraperitoneal to the rats for two weeks:

• Group 1 (n = 10): Control group (distilled water only),

• Group 2 (n = 10): Acetamiprid group (daily, 10 mg/kg acetamiprid),

• Group 3 (n = 10): *S. veneris* extract (SvE) group (daily, 100 mg/kg SvE),

• Group 4 (n = 10): CeO_2-NPs/SvE group (daily, 100 mg/kg CeO_2-NPs/SvE),

• Group 5 (n = 10): Acetamiprid + SvE group (daily, 10 mg/kg acetamiprid and 100 mg/kg SvE),

• Group 6 (n = 10): Acetamiprid + CeO_2-NPs/SvE group (daily, 10 mg/kg acetamiprid and 100 mg/kg CeO_2-NPs/SvE).

Preparation of samples. At the end of the study, the rats were anesthetized with ketamine-xylazine (50 mg/kg, 5 mg/kg) and euthanized by cervical dislocation. The blood samples were collected after euthanization. The whole blood was centrifuged at 4000 rpm for 5 minutes to extract the serum, which was then stored in the freezer at –80°C for biochemical analysis. Liver and kidney tissues were removed immediately after blood collection, washed with saline, and stored at –20°C until further analysis. The tissues were weighed and homogenized with a cold 0.15 M KCl solution in a tissue homogenizer (Magna Lyser, Roche, Switzerland) to prepare 10% homogenates (w/v). To obtain the post-mitochondrial fraction, the tissue homogenates were first centrifuged at 600 rpm for 10 minutes in a cold centrifuge set at 4°C. The resulting supernatant was then centrifuged at 10,000 rpm in an Eppendorf centrifuge for 20 minutes, and the supernatant was stored in the freezer at –80°C. The preparation of lipid extracts for measuring cholesterol and triglyceride levels followed the method described by Kolac et al. (18). Specifically, 0.25 ml of 10% tissue homogenates were mixed with 3.75 ml of chloroform: methanol solution (2 : 1), thoroughly processed, and filtered. The final volume was adjusted to 4 ml, and the samples were stored in capped tubes at –4°C until the experiments were carried out.

Histopathological analysis. For histopathological analysis, liver and kidney tissues taken from rats were fixed in a 10% buffered formaldehyde solution. Next, these tissues were routinely blocked in paraffin by passing through graded alcohol series, methyl benzoate, and benzol. Serial tissue sections of 5 µm were taken from the blocks and stained with hematoxylin and eosin. Then, one drop of entellan was added to the tissue section, and the preparations were examined under a light microscope (Zeiss Primo Star), investigating the histopathological changes.

Determination of biochemical parameters in blood. The renal and liver functions in rats were assessed using the autoanalyzer (Abbott Architect C8000, IL, USA) and commercial kits (Advia Chemistry). To evaluate renal functions, serum creatinine (CRE), uric acid, and blood urea nitrogen (BUN) were measured. Aspartate aminotransferase (AST), alanine aminotransferase (ALT), and total bilirubin (TB) were also measured to determine liver functions in rats.

The corresponding reagent kits measured glucose, cholesterol, and triglycerides (TG). The triglyceride and cholesterol levels were determined in sera. 1 ml of serum was taken, and the water phase evaporated in a boiling bath. Next, 0.4 ml of ethanol : diethyl ether (3 : 1) was added and mixed thoroughly with a vortex. Then, 0.06 ml of this extract was mixed with 0.6 ml of cholesterol and 0.6 ml of reagents from the kits used for triglyceride determinations. The tubes were kept at 37°C for 5 minutes, and the resulting color was read at 505 nm using a spectrophotometer. The results were reported as mg cholesterol/dl and mg triglycerides/dl.

Analysis of antioxidant status in liver and kidney tissues. The levels of malondialdehyde (MDA) and glutathione (GSH), as well as the activities of superoxide dismutase (SOD) and glutathione peroxidase (GSH-Px), were measured in the liver and renal tissues of rats. MDA and GSH levels were determined in tissue homogenates of 10% (w/v) prepared at 0.15 M KCl of tissues. SOD and GSH-Px activities were determined in the post-mitochondrial fraction obtained by gradual centrifugation from liver and kidney homogenates.

Assessment of lipid peroxidation in tissues. Lipid peroxidation levels were estimated using the colorimetric thiobarbituric acid reactive substance (TBARS) method (18). A total of 0.2 ml of liver or kidney tissue homogenates were taken and mixed with 0.2 ml of 8.1% sodiumdodecylsulfate, 1.5 ml of 20% acetic acid, 1.5 ml of 0.8% TBA, and 0.6 ml of distilled water. The mixture was then incubated in a water bath at 90°C for 60 minutes. After incubation, the mixture was rapidly cooled on ice. Then, 1 ml of distilled water and 5 ml of butanol/pyridine mixture (15 : 1) were added. The mixture was centrifuged at 1000 rpm for 10 minutes to separate the organic phase. The supernatant's optical density was measured at 532 nm using a UV spectrophotometer, with 1,1,3,3-tetraethoxypropane as the standard. The results were presented as pmol/mg protein.

Measurement of glutathione (GSH) levels. GSH levels were measured using the Elman reagent (5,5'-dithiobis-2 nitro benzoic acid). This reagent is reduced by free sulfhydryl (-SH) groups in tissues, resulting in the formation of 1 mole of 2-nitro-5 thiobenzoic (DTNB) acid for every 1 mole of SH group (19). For the analysis, 0.5 ml of liver or 1 ml of kidney tissue homogenates was taken, and the volumes were adjusted to 2 ml with 0.15M KCl. 3 ml of deproteinizing solution (sodium chloride, metaphosphoric acid, EDTA, and distilled water) was added to the mixture and centrifuged at 3000 rpm for 10 minutes. Next, 0.5 ml of the supernatant was combined with 2 ml of 0.3 M Na_2HPO_4 and 0.5 ml of Elman reagent. A UV spectrophotometer measured the resulting yellow product for absorbance at 412 nm. GSH levels were calculated using an extinction coefficient of 13600 $M^{-1} \times cm^{-1}$, and the results were expressed as nmol GSH/mg protein.

Measurement of superoxide dismutase (SOD) activity. The activity of SOD is measured by the ability of riboflavin-sensitized o-ranitidine to increase the rate of photooxidation. The superoxide radical, formed by the fluorescence effect of riboflavin, is converted into hydrogen peroxide in the presence of SOD. Hydrogen peroxide reacts with o-dianicidinin to produce a colored product, which is then detected spectrophotometrically (18, 28, 36). 2.6 ml of 50 mM potassium phosphate buffer (pH 7.8) and 0.1 ml of o-dianicide were added to the blind, standard, and test tubes, respectively. In the blind tube, 0.1 ml of distilled water was added, while in the standard tube, 0.1 ml of SOD standard (Sigma) was added. In the test tube, the post-mitochondrial fraction (0.05 ml for the liver, 0.1 ml for the kidney) was added, followed by 0.2 ml of riboflavin to each tube, 30 seconds apart. The absorbance values at 460 nm were then determined spectrophotometrically. The tubes were placed in a special box 37°C containing a 20 W fluorescence lamp for 8 minutes. At the end of the period, the tubes' absorbance was measured again, and the difference between the two readings was calculated. The same procedures were carried out for the experimental blind and the standard.

Measurement of glutathione peroxidase (GSH-Px) activity. GSH-Px activity determination involves two reactions (19). The first reaction reduces hydrogen peroxide (H_2O_2) or organic hydroperoxide by GSH-Px while converting GSH in the environment to oxidized GSH (GSSG). The second reaction oxidizes GSSG to GSH by GSH-reductase (GSH-R) and converts nicotine amide adenine dinucleotide (NADPH) to $NADP^+$. GSH-Px activity was measured in a prepared medium containing 50 mM potassium phosphate buffer (pH 7.0), one mM EDTA, 1 mM sodium azide, 0.2 mM NADPH, one mM GSH, 0.5 IU/ml glutathione reductase, and 1.2 mM cumene hydroperoxide. The post-mitochondrial fraction of the liver was diluted 50 times, and 0.05 ml was added to the medium. The post-mitochondrial fraction of the kidney was diluted fivefold, and 0.02 ml was added to the medium for renal GSH-Px determination. The cuvettes were placed on a spectrophotometer with a thermostat set to 37°C, and the absorbance change at 340 nm was observed at 1-minute intervals. Additionally, a non-enzymatic change was recorded by monitoring the reaction in the medium without the post-mitochondrial fraction (blind experiment). GSH-Px activity was determined by calculating the results using the extinction coefficient of NADPH ($6.22 \times 103\ M^{-1} \times cm^{-1}$) and expressed in nmol NADPH/mg protein/minute.

Protein determination. The protein content of tissue homogenates and post-mitochondrial fractions was determined using the bi-iconic acid method described by Smith et al. (32). The protein colorant reagent was prepared by adding 0.2 ml of 4% $CuSO_4$ to 10 ml of Biticinchoninic acid solution (Sigma). 200 µl of the protein colorant reagent was taken, and 10 µl was added from diluted liver or kidney homogenates or post-mitochondrial fractions. The sample was allowed to cool to room temperature before measuring its absorbance spectrophotometrically at 562 nm.

Determination of anti-inflammatory effects of SvE and CeO_2-NPs/SvE. To investigate the anti-inflammatory effects of SvE and CeO_2-NPs/SvE *in vivo*, Enzyme-Linked Immune Sorbent Analyses (ELISA) tests were performed using liver or kidney homogenates that were frozen at –80°C before analysis and then thawed on ice. The levels of the pro-inflammatory cytokines, tumor necrosis factor-alpha (TNF-α), and interleukin-6 (IL-6) were determined using Sandwich-ELISA rat kits (E-bioscience, San Diego, CA, USA). The levels of the anti-inflammatory immunomodulatory mediators, interleukin-10 (IL-10) and transforming growth factor-β (TGF-β), were measured using Sandwich-ELISA rat kits (E-bioscience, San Diego, CA, USA). Following the manufacturer's instructions, ELISA plates were pre-coated with specific antibodies to TNF-α, IL-6, IL-10, or TGF-β. Tissue homogenates from animals were diluted by 1/2 and included in ELISA analyses. The ELISA results were determined using a microplate reader (Epoch 2 Microplate Spectrophotometer, BioTek, USA). The Gen5 Microplate data connection and analysis software analyzed the microplate data.

Statistical analysis. This was conducted using SPSS 25.0 software. Data were analyzed and compared using one-way analysis of variance (ANOVA) followed by post-hoc Tukey's test. A significance level of $P < 0.05$ was used. The data are presented as mean ± standard deviation (SD).

Ethical approval. All procedures performed in this study were according to the ethical standards of the institutional and national research committee, along with the 1964 Helsinki Declaration and its later amendments or comparable ethical standards. The authors of this article carried out animal studies. The study was approved by the Girne American University ethics committee (2023/033).

Results and discussion

Phenolic compounds contain at least one phenol unit and hydroxyl substituents. They are secondary metabolites found in plants, providing unique flavor compounds and benefits such as protection against pathogens and UV rays. Previous scientific studies have shown that phenol-rich plant extracts possess antimicrobial, antioxidant, and anti-inflammatory properties, which can help reduce the risk of chronic diseases and cancer (18, 33, 36). The total polyphenolic content of the SvE was found to be 100.84 ± 0.12 mg GA/g extract, also calculated per gram of sample using the same method. The concentration of flavonoid compounds in SvE was found its level 144.22 ± 1.28 mg quercetin/g SvE. The *S. veneris* extract's total saponin content was 72.51 ± 0.76 mg oleanolic acid/g extract.

Quantification and identification of phenolic compounds in SvE were performed using HPLC. Twenty-two phenolic compounds were identified, including apigenin, caffeic acid, catechin, coumarin, coumaric acid, ferulic acid, gallic acid, kaempferol, luteolin, myricetin, rosmarinic acid, rutin, sinapic acid, syringic acid, tannic acid, trans-cinnamic acid, and vanillic acid. The values were expressed as µg/g SvE (see Fig. 1 and Tab. 1).

Tab. 1. Quantification and identification of phenolic compounds in SvE*

Compounds	Quantification (mg analyte/g extract)	Peak/Retention time
Rosmarinic acid	34.9 ± 13.4	9/24.9
Isoquercitrin	32.45 ± 0.5	13/30.5
Acacetin	20.52 ± 0.7	14/35.6
Naringenin	14.22 ± 0.4	17/36.5
Fumaric acid	10.21 ± 0.12	2/3.9
Protocatechuic acid	5.73 ± 0.08	3/6.8
Luteolin	3.85 ± 0.08	19/38.3
Caffeic acid	0.813 ± 0.03	6/12.1
Quinic acid	0.726 ± 0.32	1/3.0
Cosmosiin	0.357 ± 0.03	10/25.5
Cynaroside	0.251 ± 0.04	8/23.7
Protocatechuic aldehyde	0.247 ± 0.01	5/8.5
Chlorogenic acid	0.127 ± 0.04	4/8.4
Hesperidin	0.115 ± 0.009	11/25.7
Astragalin	0.082 ± 0.005	22/40.9
Salicylic acid	0.056 ± 0.005	7/21.8
Nicotiflorin	0.035 ± 0.003	15/35.8
Apigenin	0.027 ± 0.003	21/39.0
Genistein	0.018 ± 0.003	20/38.5
Rutin	0.011 ± 0.002	12/30.3
Quercetin	0.010 ± 0.001	16/36.0
Hesperetin	0.005 ± 0.0007	18/37.0

Explanation: * The mean values ($\bar{x}$) were obtained from three parallel measurements and are expressed as $\bar{x}$ ± SD.

In this study, we synthesized CeO_2-NPs/SvE from *S. veneris* using cerium nitrate as the precursor. We controlled the synthesis and catalytic activity of CeO_2-NPs/SvE using various techniques such as UV spectroscopy, FTIR, XRD, and SEM (18).

The formation of CeO_2-NPs/SvE was confirmed by analyzing the absorbance values at 360-370 nm using a UV spectrophotometer (2). Our study's peak value, 367 nm, supported the synthesis of CeO_2-NPs/SvE (Fig. 2A). The FTIR spectrum of CeO_2-NPs/SvE is shown in Fig. 2B. Comparative FTIR results reveal significant absorption peaks in the wavenumber range of 400-4000 cm^{-1} (24). The absorption band of the biomolecules of *S. veneris* extract peaks at 680 cm^{-1} (C-H), 1030 cm^{-1} (C-O), 1570 cm^{-1} (O-H bending vibration), 1710 cm^{-1} (C=C), 2964 cm^{-1} (N-H), and 3260 cm^{-1}

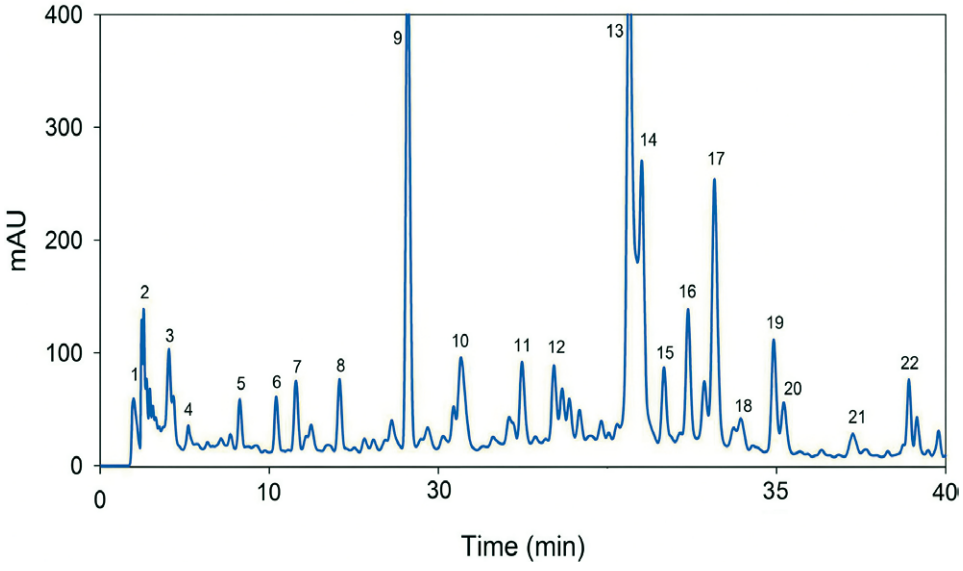

Fig. 1. The HPLC chromatograms of *S. veneris* extract (SvE) ranged from 280-400 nm

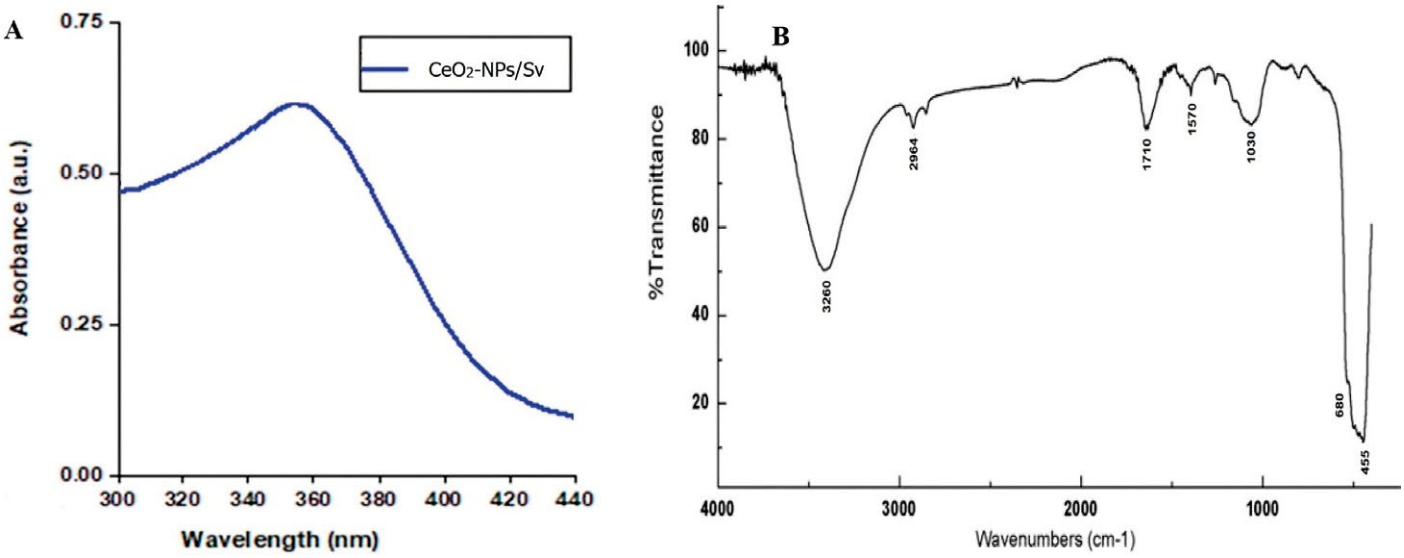

Fig. 2. A. The UV spectrum shows the synthesis of CeO_2-NPs using *S. veneris* extract at various time intervals. The absorbance curve is displayed in blue. Our study found peak values of 367 nm, supporting the synthesis of CeO_2-NPs/SvE; B. The FTIR of CeO_2-NPs/SvE was obtained from *S. veneris* extract

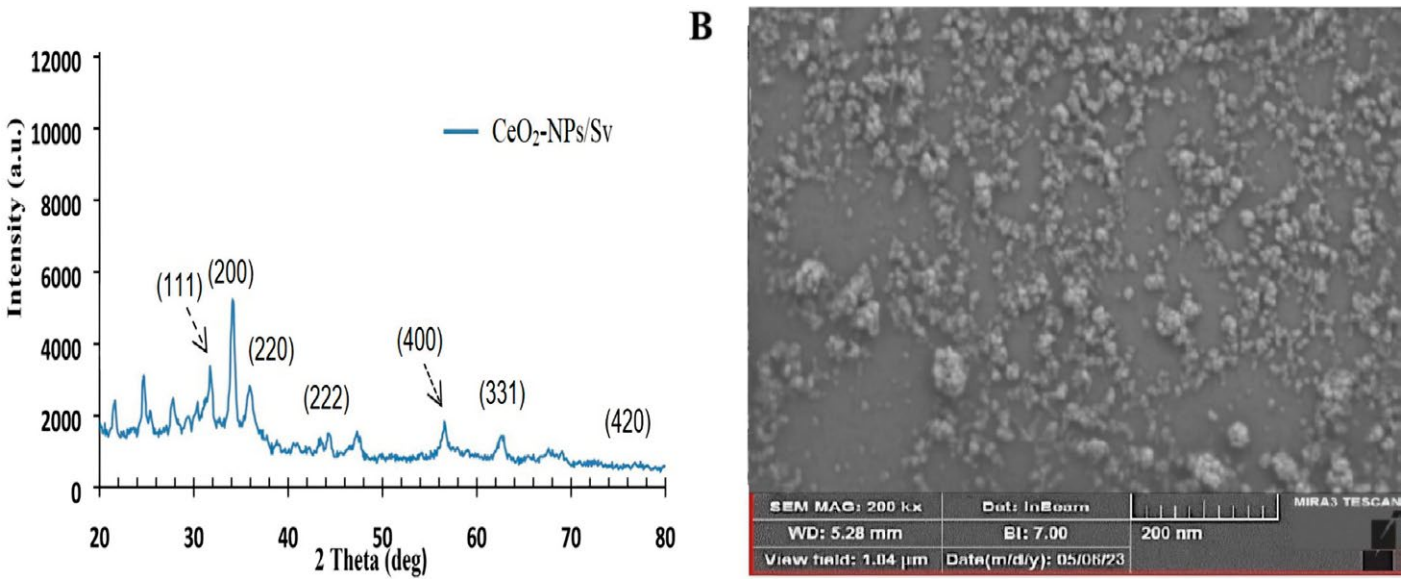

Fig. 3. A. The XRD pattern shows the CeO_2-NPs/SvE was obtained from *S. veneris* extract; B. The SEM image of the CeO_2-NPs/SvE was obtained from *S. veneris* extract

(O-H tensile vibration). In our study, we measured the spectra resulting from the stretching frequency of Ce-O, which were found to be 455 cm^{-1}, indicating the fabrication of CeO_2-NPs/SvE.

The zeta potential test assessed the electric charge on the surface of CeO_2-NPs/SvE. At the same time, the crystal structure of the synthesized CeO_2-NPs/SvE was revealed through XRD analysis (18) (Fig. 3A). The figure shows peaks denoted by values of 2θ, including 38.64, 33.04, 47.52, 56.61, 69.38, 75.96 and 78.84, which correspond to (111), (200), (220), (222), (400), (331) and (420), respectively. The SEM images revealed particles with rounded morphologies and an average size of 200 µm (18) (see Fig. 3B).

Normal histological findings are seen in the control group's rat liver and kidney tissue samples. The typical liver tissue structure in the control group depicts a normal shape and arrangement of hepatocytes and sinusoidal spaces (Fig. 4A). In the CeO_2-NPs/SvE-treated group, normal histological features of hepatic tissues with only mild congestion were observed (Fig. 4B, 4C). In the Acetamiprid + SvE group, the typical architecture of liver tissue with only mild congestion was observed (Fig. 4D). In the group administered 10 mg/kg acetamiprid, vacuolation in hepatocytes, pyknosis in cell nuclei, and congestion in liver tissue were observed (Fig. 4E, 4F). In the control group, renal tubules are embedded in the parenchyma among normal-shaped kidney cells, erythropoietic and granulopoietic series, lymphocytes, and phagocytes in this area. The space between kidney cells is quite narrow (Fig. 5A). When kidney histology was examined in the Acetamiprid + CeO_2-NPs/SvE group, despite slight degeneration in the distal tubules and increased capsule area, the

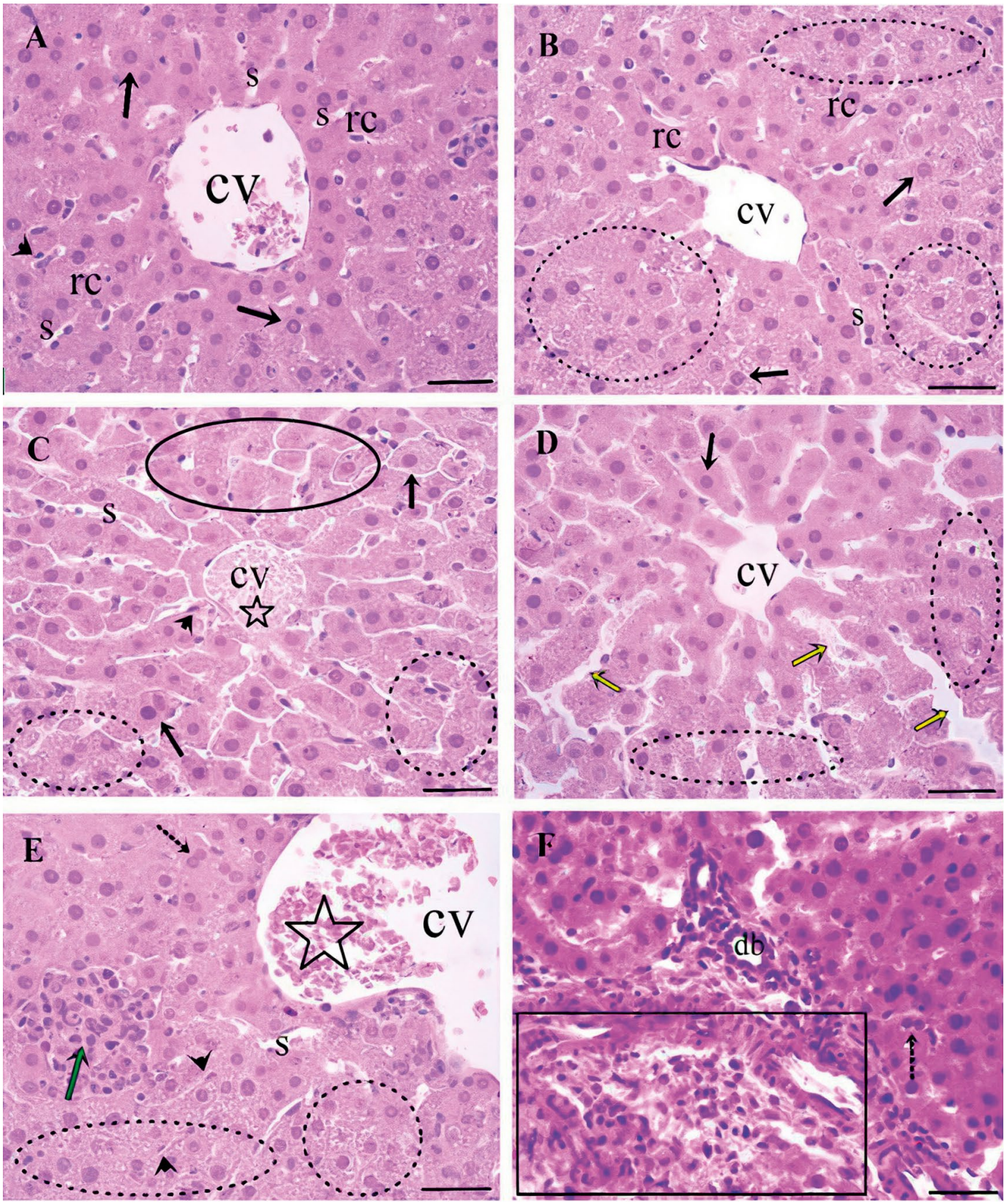

Fig. 4. A. Normal liver histology of control group; B, C. Histological structure of the liver in the Acetamiprid + CeO_2-NPs/ SvE group; D. Histological structure of the liver in the Acetamiprid + SvE group; E, F. Histological structure of the liver in the 10 mg/kg Acetamiprid group

Explanations: cv – central vena; rc – radially arranged remark cords; s – sinusoid; black arrow – hepatocytes; black arrowhead – Kupffer's star cell; dashed circle – microvesicular steatosis in hepatocytes; asterisk – congestion in the central vein; black circle – degeneration, necrotic areas and steatosis in hepatocytes; yellow arrow – sinusoidal dilation; green arrow – inflammatory cell infiltration; rectangular area – vacuolar and hepatocellular degeneration in the parenchymal region; dashed arrow – regenerative binuclear hepatocytes; db – ductus biliferi; H&E; bar – 50 µm

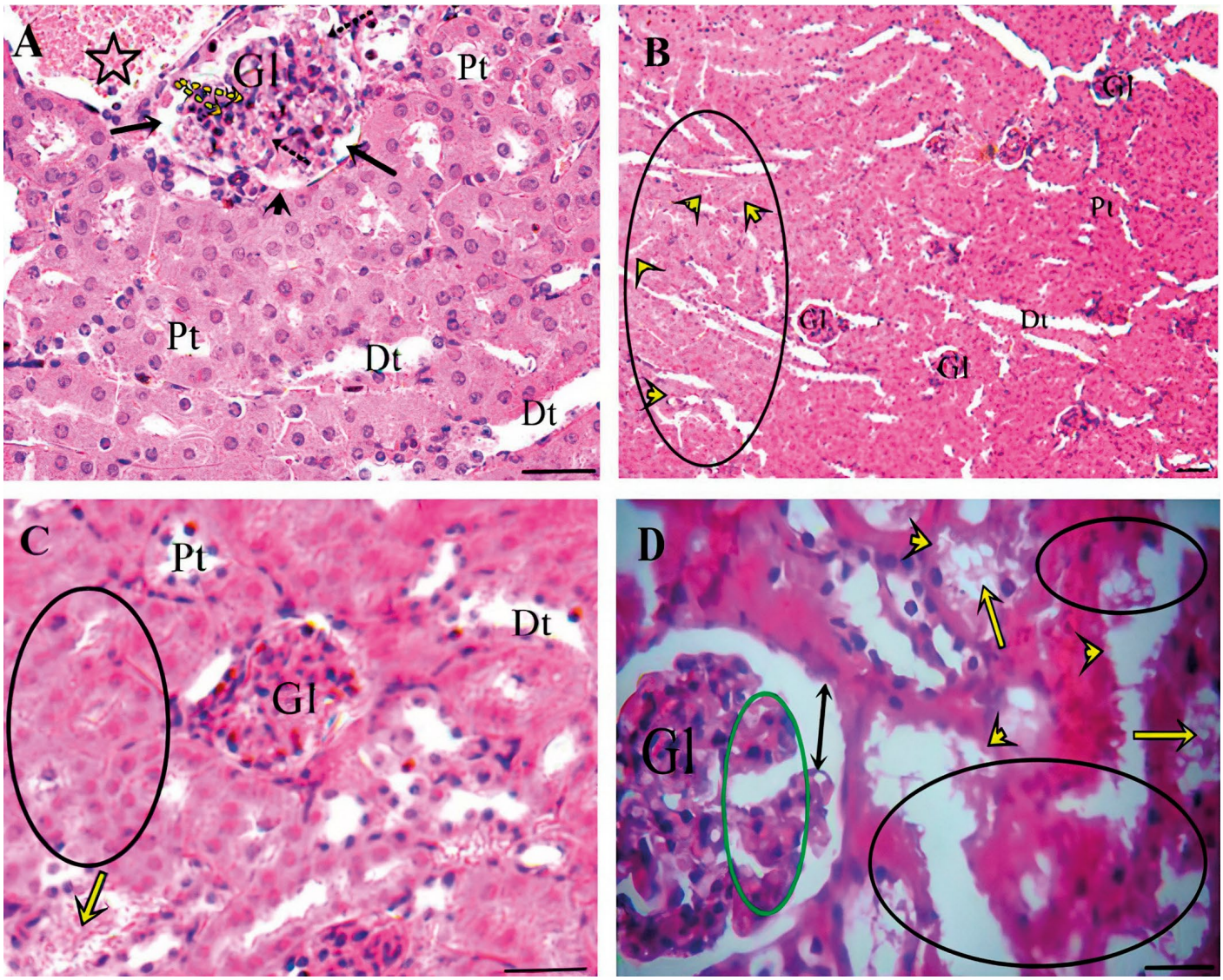

Fig. 5. A. Normal kidney histology of the control group; B. Histological structure of the kidney in the Acetamiprid + CeO_2-NPs/SvE group; C. Histological structure of the kidney in the Acetamiprid + SvE group; D. Histological structure of the kidney in the 10 mg/kg Acetamiprid group

Explanations: Gl – glomeruli; Pt – proximal tubule; Dt – distal tubule; black arrowhead – bowman's capsule; black arrow – bowman's space; dashed black arrow – glomerular capillaries; dashed yellow arrow – mesangial cells; asterisk – vein; yellow arrowhead – degenerate tubule epithelial cells; black circle – diffuse tubular degeneration; yellow arrow – intratubular cast; green circle – glomerular lobulation; double-sided arrowhead – enlargement of bowman space

general appearance was similar to that of the control group (Fig. 5B). In the Acetamiprid + SvE group, the degeneration in the distal tubules increased even more and reached necrotic dimensions (Fig. 5C). In the group administrated 10 mg/kg acetamiprid, glomerular degeneration and atrophy, an appearance without a Bowman capsule due to the glomerulus filling the Bowman capsule, hemorrhage, and necrosis in the tubules was observed (Fig. 5D).

This study aimed to investigate the antioxidant, anti-inflammatory, nephroprotective, and hepatoprotective properties of *S. veneris* plant extract and the synthesized CeO_2 nanoparticles of *S. veneris* (CeO_2-NPs/SvE) on acetamiprid-induced hepatotoxicity and nephrotoxicity in rats. The primary biochemical parameters in serum were determined in rats, including serum CRE, uric acid, BUN, AST, ALT, TB, serum glucose, cholesterol, and triglyceride levels. The antioxidant status was determined in the liver and kidney tissues of rats with acetamiprid-induced oxidative stress by levels of MDA and GSH, as well as SOD and GSH-Px activities. To investigate the anti-inflammatory effects of *S. veneris* and CeO_2-NPs/SvE *in vivo*, we measured the levels of pro-inflammatory cytokines TNF-α and IL-6, as well as anti-inflammatory cytokines IL-10 and TGF-β in liver and kidney tissue homogenates using ELISA rat kits (Tab. 2).

Throughout human history, people all over the world have used plant-based medicines. Today, complementary medicine is an integral part of the health care system for the treatment of disease. However, they must be scientifically researched and used appropriately

Tab. 2. The effects of *S. veneris* extract and CeO_2-NPs/SvE on serum biochemical parameters, antioxidant, and anti-inflammatory activities in rats with acetamiprid-induced hepatotoxicity and nephrotoxicity*

Group	Biochemical parameters								
	Creatinine (mg/dL)	Uric acid (mg/dL)	Urea (mg/dL)	AST (IU/L)	ALT (IU/L)	TB (mg/dL)	Glucose (g/dL)	Cholesterol (mg/dL)	TG (mg/dL)
Control	0.29 ± 0.03	0.18 ± 0.02	32.94 ± 0.07	26.7 ± 1.7	122.4 ± 5.8	1.24 ± 0.1	6.45 ± 0.2	53.4 ± 1.7	100.7 ± 3.8
Acetamiprid	0.57 ± 0.05^{a}	0.32 ± 0.03^{a}	58.57 ± 0.09^{a}	45.7 ± 2.9^{a}	162.7 ± 9.2^{a}	1.82 ± 0.8^{a}	5.83 ± 0.5^{a}	100.3 ± 3.5^{a}	195.8 ± 4.2^{a}
SvE	0.42 ± 0.03^{ab}	0.28 ± 0.02^{a}	40.18 ± 0.08^{ab}	30.4 ± 3.2^{ab}	139.1 ± 4.8^{ab}	1.38 ± 0.6^{ab}	6.21 ± 0.4^{ab}	86.5 ± 4.3^{ab}	146.3 ± 2.4^{ab}
CeO_2-NPs/SvE	0.48 ± 0.04^{ab}	0.26 ± 0.05^{ab}	38.02 ± 0.22^{ab}	28.3 ± 4.2^{ab}	138.2 ± 5.2^{ab}	1.36 ± 0.2^{ab}	6.35 ± 0.2^{ab}	82.3 ± 5.2^{ab}	148.4 ± 3.7^{ab}
Acetamiprid+SvE	0.39 ± 0.03^{ab}	0.24 ± 0.05^{b}	46.17 ± 0.06^{b}	36.3 ± 3.2^{ab}	145.2 ± 6.6^{ab}	1.42 ± 0.9^{ab}	6.05 ± 0.7^{ab}	68.21 ± 3.8^{ab}	119.2 ± 4.1^{b}
Acetamiprid+CeO_2-NPs/SvE	0.35 ± 0.03^{ab}	0.23 ± 0.01^{b}	44.58 ± 0.05^{b}	34.3 ± 3.4^{b}	141.5 ± 3.5^{ab}	1.40 ± 0.3^{ab}	6.23 ± 0.2^{ab}	64.47 ± 4.2^{ab}	113.6 ± 3.3^{b}

Group	Antioxidants							
	MDA (pmol/mg)		GSH (nmol/mg)		SOD (U/mg)		GSH-Px (nmol/dk/mg)	
	Liver	Kidney	Liver	Kidney	Liver	Kidney	Liver	Kidney
Control	515.2 ± 12.4	527.6 ± 32.1	35.43 ± 1.3	38.52 ± 3.2	73.27 ± 4.7	57.35 ± 3.8	721.3 ± 27.2	682.7 ± 21.9
Acetamiprid	631.2 ± 25.3^{a}	628.5 ± 33.4^{a}	19.27 ± 2.8^{a}	22.14 ± 1.7^{a}	55.16 ± 5.5^{a}	36.87 ± 3.1^{a}	578.3 ± 27.5^{a}	551.9 ± 45.6^{a}
SvE	527.5 ± 23.1^{b}	532.2 ± 21.7^{b}	37.58 ± 3.3^{ab}	35.27 ± 2.8^{ab}	76.51 ± 5.3^{ab}	66.32 ± 4.8^{ab}	735.5 ± 54.3^{b}	762.3 ± 54.1^{b}
CeO_2-NPs/Sv	536.9 ± 22.4^{bc}	548.7 ± 23.6^{b}	38.22 ± 2.5^{b}	36.18 ± 3.5^{b}	77.32 ± 6.4^{ab}	70.57 ± 5.3^{ab}	742.6 ± 37.1^{b}	688.5 ± 18.7^{b}
Acetamiprid + SvE	540.6 ± 23.1^{ab}	554.8 ± 22.5^{ab}	30.52 ± 3.1^{ab}	31.71 ± 2.7^{ab}	68.41 ± 5.8^{ab}	46.81 ± 3.6^{ab}	684.2 ± 47.3^{ab}	654.8 ± 37.8^{ab}
Acetamiprid + CeO_2-NPs/SvE	530.3 ± 22.2^{ab}	540.1 ± 34.3^{ab}	32.75 ± 2.9^{ab}	32.42 ± 1.8^{ab}	69.92 ± 3.2^{ab}	49.28 ± 4.3^{ab}	690.5 ± 52.7^{ab}	660.3 ± 21.7^{ab}

Group	Cytokines							
	TNF-α (pmol/mL)		IL-6 (pmol/mL)		IL-10 (pmol/mL)		TGF-β (pmol/mL)	
	Liver	Kidney	Liver	Kidney	Liver	Kidney	Liver	Kidney
Control	71.4 ± 5.4	75.6 ± 2.6	25.52 ± 2.9	28.37 ± 4.3	121.2 ± 10.2	125.3 ± 12.7	618.2 ± 31.3	642.5 ± 33.7
Acetamiprid	161.6 ± 4.3^{a}	158.2 ± 5.1^{a}	39.12 ± 3.5^{a}	42.82 ± 5.2^{a}	83.8 ± 8.2^{a}	88.4 ± 9.2^{a}	296.2 ± 29.4^{a}	367.5 ± 35.2^{a}
SvE	81.2 ± 5.3^{b}	92.7 ± 5.4^{b}	28.92 ± 4.3^{ab}	35.18 ± 3.9^{ab}	117.6 ± 10.1^{b}	112.3 ± 11.2^{b}	547.2 ± 32.5^{b}	562.7 ± 19.8^{b}
CeO_2-NPs/Sv	79.3 ± 3.4^{b}	91.3 ± 4.8^{b}	29.57 ± 4.8^{ab}	36.47 ± 4.2^{b}	115.7 ± 9.7^{b}	115.6 ± 7.5^{b}	562.8 ± 42.6^{b}	588.6 ± 32.5^{b}
Acetamiprid + SvE	76.3 ± 3.9^{ab}	80.9 ± 5.1^{ab}	28.34 ± 2.8^{ab}	33.02 ± 4.6^{ab}	114.7 ± 8.2^{ab}	109.3 ± 6.2^{ab}	582.1 ± 32.5^{ab}	612.3 ± 23.4^{ab}
Acetamiprid + CeO_2-NPs/SvE	75.9 ± 3.8^{ab}	78.6 ± 3.5^{ab}	27.12 ± 1.6^{ab}	31.11 ± 3.6^{ab}	118.3 ± 7.6^{ab}	111.8 ± 8.6^{ab}	593.2 ± 27.2^{ab}	624.8 ± 32.8^{ab}

Explanations: * Values are expressed as $\bar{x} \pm SD$; a – significant versus control group; b – significant versus Acetamiprid group; $p \leq 0.05$ are significantly different at one-way ANOVA followed by Tukey's test.

for the specific disease, dose, and mode of use. Plants contain phytochemicals, which are active ingredients with beneficial properties for treating many diseases. Compounds found in plants, such as terpenoids, phytosterols, flavonoids, alkaloids, carotenoids, phenols, organic acids, and protease inhibitors, play important roles in human health. ROS are produced in the body during normal cellular metabolism and can contribute to the development of chronic diseases. ROS are highly reactive and can easily damage cells during biochemical reactions, leading to lipid peroxidation. This is important in developing chronic diseases (9, 10, 14). Nanoparticles synthesized from plants effectively bind FOR, hydroxyl radicals, hydrogen peroxide, superoxide anion radicals, and singlet oxygen, reducing oxidative stress. According to Nadeem et al. (22), medicinal plants with high levels of antioxidant phytochemicals, such as phenols, tannins, and flavonoids, have been observed to enhance their lipid peroxidation-inhibiting effects through synthesis with CeO_2. *Salvia* spp. have been found to protect against various chronic diseases, including cancer, cardiovascular and cerebrovascular diseases, atherosclerosis, and diabetes. This may be due to their high antioxidant capacity (18, 36). Recent research has shown that antioxidants and anti-inflammatory agents have potential value in treating dyslipidemia, hyperglycemia, increased oxidative stress, cardiovascular disease, cancer, diabetes, dementia, and other age-related diseases. However, only a few studies investigating the interaction of biochemical and anti-inflammatory parameters with *Salvia veneris* have been found in the literature (18, 22, 36). The present study is the first to investigate the effect of synthesized CeO_2 nanoparticles of *S. veneris*.

Quantification and identification of phenolic compounds in SvE were performed using HPLC. The sample contains a range of phenolic compounds, especially rosmarinic acid (34.9 ± 13.4 mg/g), the most abundant. High levels of fumaric acid (10.21 ± 0.12 mg/g), acacetin (20.52 ± 0.7 mg/g), isoquercitrin (32.45 ± 0.5 mg/g), and naringenin (14.22 ± 0.4 mg/g) were detected in SvE. In a study by Bakir et al. (6) on *S. hypargeia* leaf extract, the amount of rosmarinic acid was found to be 38.04 mg/g, and isoquercitrin was found to be 4.14 mg/g. Bursal et al. (8) identified major compounds in *S. eriophora Boiss&Kotschy's* water extract, including fumaric acid (0.555 ± 0.038 mg/g), caffeic acid (0.103 ± 0.02 mg/g), and epicatechin (0.083 ± 0.008 mg/g). Yilmaz et al. (36) also detected high levels of phenolic (rosmarinic acid and caffeic acid) and flavonoid compounds (luteolin, naringenin, and acacetin) in *S. aytachii*. These findings are in agreement with our results.

In this study, we controlled the synthesis and catalytic activity of CeO_2-NPs/SvE using various techniques, such as UV spectroscopy, FTIR, XRD, and SEM. Analyzing those techniques confirmed the formation of CeO_2-NPs/SvE in accordance with previous studies (4, 5, 21).

In the histopathological analysis of liver and kidney tissues, it was observed that the group receiving 10 mg/kg acetamiprid showed vacuolation in hepatocytes, pyknosis in cell nuclei, congestion in liver tissue, glomerular degeneration, and atrophy, a glomerulus filling the Bowman capsule, as well as hemorrhage and necrosis in the kidney tissue tubules. These findings were consistent with previous studies (14, 25). Our study revealed that pre-treating rats with *S. veneris* extract and CeO_2-NPs/SvE resulted in slight and significant improvements in all observed histopathological parameters compared to the acetamiprid group.

The main biochemical parameters we analyzed in rats. The administration of acetamiprid (10 mg/kg) resulted in a significant decrease in glucose levels and an increase ($p \leq 0.05$) in all other biochemical parameters compared to the control and other groups. Pre-treatment of rats with *S. veneris* extract and CeO_2-NPs/SvE at 100 mg/kg significantly increased glucose levels. They reduced all measured biochemical parameters compared to the acetamiprid group ($p \leq 0.05$). However, rats pretreated with 100 mg/kg CeO_2-NPs/SvE showed insignificantly higher glucose levels and lower levels of all other biochemical parameters than the 100 mg/kg acetamiprid + SvE group. Antioxidant markers have long been used in studies of oxidative stress and the antioxidant effects of plants. The administration of acetamiprid significantly increased hepatic and renal levels of MDA while reducing levels of the hepatic and renal antioxidants GSH, SOD, and GSH-Px. Using *S. veneris* extract and CeO_2-NPs/SvE significantly decreased the acetamiprid-induced elevation of liver and kidney tissue content of MDA, a marker of lipid peroxidation. Furthermore, the extract of *S. veneris* and CeO_2-NPs/SvE significantly increased the hepatic and renal tissue content of GSH, SOD, and GSH-Px, which are important antioxidant defenses of human tissues. Previous studies have demonstrated that the methanolic extracts of *Salvia* spp. can scavenge 2,2-Diphenyl-1-picryl hydrazyl (DPPH) free radicals and exhibit total antioxidant activity. Additionally, these extracts have been shown to resist oxidative stress caused by H_2O_2 in astrocytes by scavenging FOR and blocking the H_2O_2-induced mitogen-activated protein kinase (MAPK) pathway (27, 28). The studies revealed high levels of phenolic and flavonoid compounds in the *Salvia* spp. extracts. Furthermore, the sage extract increases resistance to oxidative stress in the liver cells of experimental animals by increasing GSH-Px activity and GSH content in rats and reducing DNA damage caused by oxidants (15). Consistent with our findings, in a lipopolysaccharide-induced experimental inflammation model, significantly higher levels of MDA in erythrocytes and liver, lung, and kidney tissues of rats has also been observed compared to the

group administered *S. officinalis* extract. Additionally, the activities of SOD, CAT, and GSH-Px, as well as erythrocyte SOD and CAT activities in liver, lung, and kidney tissues, were significantly lower in the group that did not receive *S. officinalis* extract (18).

To investigate the anti-inflammatory effects of *S. veneris* and CeO_2-NPs/SvE *in vivo*, we measured the levels of pro-inflammatory cytokines TNF-α and IL-6, as well as anti-inflammatory cytokines IL-10 and TGF-β in liver and kidney tissue homogenates using ELISA rat kits. We found that TNF-α and IL-6 levels were significantly increased in the liver and kidney tissue homogenates of rats administered with acetamiprid compared to the normal group. Treatment of rats with hepatotoxic and nephrotoxic effects induced by acetamiprid was carried out using *S. veneris* extract and CeO_2-NPs/SvE. The results showed a significant reduction in TNF-α and IL-6 levels. CeO_2-NPs/SvE had a slightly greater effect than *S. veneris* extract. Furthermore, IL-10 and TGF-β levels were significantly reduced in liver and kidney tissue homogenates of the acetamiprid-treated group compared to the control group. However, the levels of anti-inflammatory markers, IL-10 and TGF-β cytokines, significantly increased in acetamiprid-induced hepatotoxic and nephrotoxic rats treated with *S. veneris* extract and CeO_2-NPs/SvE. The effectiveness of CeO_2-NPs/SvE treatment in rats administered with acetamiprid was moderate compared to the group treated with *S. veneris* extract.

Previous studies have reported that *S. officinalis* and *S. plebian* exert anti-inflammatory effects by reducing the production of nitric oxide and prostaglandin E_2 (PGE_2) in macrophages, as well as the gene expression levels of iNOS, cytokines (IL-1a, IL-6), and chemokines (1, 26). In another study, tanshinones isolated from *S. miltiorrhiza* significantly inhibited mRNA and protein expression of TNF-α, IL-1b, and IL-8 in lipopolysaccharide-stimulated macrophages (7). Our study also confirmed that *Salvia spp.* has strong anti-inflammatory properties due to its phenolic compounds, such as isoquercitrin, fumaric acid, rosmarinic acid, and naringenin (20).

Sage is widely used in traditional medicine to treat the respiratory tract, digestive system, rheumatism, heart diseases, skin infections, gynecological diseases, and various cancers. *In vitro* and animal studies have confirmed that many Salvia species have antioxidant activity and contain many active compounds, including polyphenols, phenolics, flavonoids, sterols, terpenoids, and volatile oils that can protect against oxidative stress and many diseases. CeO_2-NPs have been synthesized as a safe and biocompatible nanomaterial by green synthesis and used in experimental studies. Our study demonstrated the antioxidant, anti-inflammatory, hepatoprotective, and nephroprotective properties of *S. veneris* plant extract and CeO_2-NPs/SvE on acetamiprid-induced hepatotoxicity and nephrotoxicity in rats. Cerium oxide nanoparticles protect cells due to their strong anti-inflammatory and antioxidant properties and radical quenching activities. Finally, further research is recommended to improve our understanding of the potential health benefits of Salvia plants.

References

1. *Akram M., Syed A. S., Kim K. A., Lee J. S., Chang S. Y., Kim C. Y.*: Heme oxygenase 1-mediated novel anti-inflammatory activities of Salvia plebeia and its active components. J. Ethnopharmacol. 2015, 4, 322-330.
2. *Allu I., Kumar Sahi A., Kumari P., Sakhile K., Sionkowska A., Gundu S.*: A brief review on cerium oxide (CeO_2NPs)-based scaffolds: recent advances in wound healing applications. Micromachines (Basel) 2023, 14, 865-873.
3. *Amiri A., Nikitina N., Stepanova L., Beregova T.*: Potential impact of cerium dioxide nanoparticles (nanoceria) on the concentration of C-reactive protein and middle-mass molecules after wound treatment in rats. Sci. Biol. Sci. 2019, 16, 14-19.
4. *Antony D., Yadav R.*: Facile fabrication of green nano pure CeO_2 and Mn-decorated CeO_2 with Cassia angustifolia seed extract in water refinement by optimal photodegradation kinetics of malachite green. Environ. Sci. Pollut. Res. Int. 2021, 28, 18589-18603.
5. *Arumugam A., Karthikeyan C., Hameed A. S. H., Gopinath K., Gowri S., Karthika V.*: Synthesis of cerium oxide nanoparticles using Gloriosa superba L. leaf extract and their structural, optical and antibacterial properties. Mater. Sci. Eng. C. Biol. Appl. 2015, 49, 408-415.
6. *Bakir D., Akdeniz M., Ertas A., Yilmaz M. A., Yener I., Firat M.*: A GC-MS method validation for quantitative investigation of some chemical markers in Salvia hypargeia Fisch. & CA Mey. of Turkey: enzyme inhibitory potential of ferruginol. J. Food Biochem. 2020, 44, 13350-13355.
7. *Bonaccini L., Karioti A., Bergonzi M. C., Bilia A. R.*: Effects of Salvia miltiorrhiza on CNS neuronal injury and degeneration: a plausible complementary role of tanshinones and depsides. Planta Med. 2015, 81, 1003-1016.
8. *Bursal E., Aras A., Kilic O., Taslimi P., Goren A. C., Gulcin I.*: Phytochemical content, antioxidant activity, and enzyme inhibition effect of Salvia eriophora Boiss. & Kotschy against acetylcholinesterase, a-amylase, butyrylcholinesterase, and a-glycosidase enzymes. J. Food Biochem. 2019, 43, 12776-12781.
9. *Caylak E., Aytekin M., Halifeoglu I.*: Antioxidant effects of methionine, alpha-lipoic acid, N-acetylcysteine and homocysteine on lead-induced oxidative stress to erythrocytes in rats. Exp. Toxicol. Pathol. 2008, 60, 289-294.
10. *Caylak E., Halifeoglu I.*: Effects of sulfur-containing antioxidants on malondialdehyde and catalase levels of liver, kidney and brain in lead-exposed rats. Tur. Klin. J. Med. Sci. 2007, 27, 1-8.
11. *Danenberg H. D., Fishbein I., Gao J., Mönkkönen J., Reich R., Gati I., Moerman E., Golomb G.*: Macrophage depletion by clodronate-containing liposomes reduces neointimal formation after balloon injury in rats and rabbits. Circulation. 2002, 106, 599-605.
12. *Dhall A., Self W.*: Cerium oxide nanoparticles: A brief review of their synthesis methods and biomedical applications. Antioxidants. 2018, 7, 97-105.
13. *Esiz Dereboylu A., Sengonca N., Guvensen A., Gucel S.*: Anatomical and palynological characteristics of Salvia willeana (Holmboe) Hedge and Salvia veneris Hedge endemic to Cyprus. Afr. J. Biotec. 2010, 9, 2076-2088.
14. *Farmer E. E., Mueller M. J.*: ROS-mediated lipid peroxidation and RES-activated signaling. Ann. Rev. Plant Biol. 2013, 64, 429-450.
15. *Horváthová E., Srančíková A., Regendová-Sedláčková E., Melušová M., Meluš V., Netriová J.*: Enriching the drinking water of rats with extracts of Salvia officinalis and Thymus vulgaris increases their resistance to oxidative stress. Mutagenesis 2016, 31, 51-59.
16. *Kanno S., Wu Y. J. L., Lee P. C., Dodd S. J., Williams M., Griffith B. P., Ho C.*: Macrophage accumulation associated with rat cardiac allograft rejection detected by magnetic resonance imaging with ultrasmall superparamagnetic iron oxide particles. Circulation. 2001, 104, 934-938.
17. *Kobyliak N., Abenavoli L., Kononenko L., Kyriienko D., Spivak M.*: Neuropathic diabetic foot ulcers treated with cerium dioxide nanoparticles: A case report. Diabetes Metab. Syndr. Clin. Res. Rev. 2019, 13, 228-234.
18. *Kolac U. K., Ustuner M. C., Tekin N., Ustuner D., Colak E., Entok E.*: The Anti-inflammatory and antioxidant effects of Salvia officinalis on lipopolysaccharide-induced inflammation in rats. J. Med. Food. 2017, 20, 1193-1200.
19. *Lawrence R. A., Burk R. F.*: Glutathione peroxidase activity in selenium-deficient rat liver. Biochem. Biophys. Res. Commun. 2012, 425, 503-509.
20. *Ma S., Zhang D., Lou H., Sun L., Ji J.:* Evaluation of the antiinflammatory activities of tanshinones isolated from Salvia miltiorrhiza var. alba roots in THP-1 macrophages. J. Ethnopharmacol. 2016, 21, 193-199.

21. *Maqbool Q., Nazar M., Naz S., Hussain T., Jabeen N., Kausar R.*: Antimicrobial potential of green synthesized CeO_2 nanoparticles from Olea europaea leaf extract. Int. J. Nanomedicine. 2016, 11, 5015-5025.
22. *Nadeem M., Khan R., Afridi K., Nadhman A., Ullah S., Faisal S.*: Green synthesis of cerium oxide nanoparticles (CeO_2-NPs) and their antimicrobial applications: a review. Int. J. Nanomedicine 2020, 15, 5951-5961.
23. *Neal C. J., Fox C. R., Sakthivel T. S., Kumar U., Fu Y., Drake C., Parks G. D., Seal S.*: Metal-mediated nanoscale cerium oxide inactivates human coronavirus and rhinovirus by surface disruption. ACS. Nano. 2021, 15, 14544-14556.
24. *Nosrati H., Heydari M., Khodaei M.*: Cerium oxide nanoparticles: synthesis methods and applications in wound healing. Mater. Today Bio. 2023, 23, 100823-100828.
25. *Nur G., Caylak E., Kilicle P. A., Sandayuk S., Celebi O. O.*: Immunohistochemical distribution of Bcl-2 and p53 apoptotic markers in acetamiprid-induced nephrotoxicity. Open Med (Wars). 2022, 17, 1788-1796.
26. *Oniga I., Parvu A. E., Toiu A., Benedec D.*: Effects of Salvia officinalis L. extract on experimental acute inflammation. Rev. Med. Chir. Soc. Med. Nat. Iasi. 2007, 111, 290-294.
27. *Pop A. V., Tofană M., Socaci S. A., Pop C., Rotar A. M., Nagy M.*: Determination of antioxidant capacity and antimicrobial activity of selected Salvia species. Bull. UASVM Food Sci. Technol. 2016, 73, 14-18.
28. *Remok F., Saidi S., Gourich A. A., Zibouh K., Maouloua M., Makhoukhi F. E.*: Phenolic content, antioxidant, antibacterial, antihyperglycemic, and α-amylase inhibitory activities of aqueous extract of Salvia lavandulifolia Vahl. Pharmaceuticals. 2023, 16, 395-399.
29. *Savi M., Rossi S., Bocchi L., Gennaccaro L., Cacciani F., Perotti A.*: Titanium dioxide nanoparticles promote arrhythmias via a direct interaction with rat cardiac tissue. Part. Fibre Toxicol. 2014, 11, 63-39.
30. *Schwager J., Richard N., Fowler A., Seifert N., Raederstorff D.*: Carnosol and related substances modulate chemokine and cytokine production in macrophages and chondrocytes. Molecules 2016, 21, 465-469.
31. *Singh K. R. B., Nayak V., Sarkar T., Singh R. P.*: Cerium oxide nanoparticles: Properties, biosynthesis and biomedical application. RSC. Adv. 2020, 10, 27194-27214.
32. *Smith P. K., Krohn R. I., Hermanson G. T., Mallia A. K., Gartner F. H., Provenzano M. D.*: Measurement of protein using bicinchoninic acid. Anal. Biochem. 1985, 150, 76-85.
33. *Toplan G. G., Kurkcuoglu M., Goger F., Iscan G., Agalar H. G., Mat A., Baser K. H. C., Koyuncu M., Sarıyar G.*: Composition and biological activities of Salvia veneris Hedge growing in Cyprus. Indus. Crops Prod. 2017, 97, 41-48.
34. *Ulker D., Abacioglu N., Sehirli A. O.*: Cerium oxide (CeO_2) nanoparticles could have protective effect against COVID-19. Lett. Appl. NanoBioScience. 2022, 12, 12-15.
35. *Xu C., Qu X.*: Cerium oxide nanoparticle: A remarkably versatile rare earth nanomaterial for biological applications. NPG. Asia Mater. 2014, 6, 90-98.
36. *Yilmaz G., Eruygur N., Bona G. E., Bona M., Akdeniz M., Yilmaz M. A.*: Phytochemical analysis, antioxidant, and enzyme inhibition activity of five Salvia taxa from Turkey. S. Afr. J. Botany. 2023, 152, 212-221.

Author's address: Dr Emrah Caylak, Firat University, Health Sciences Institute, Department of Biochemistry, Post-Doc, Elazig, Turkiye; e-mail: emrah333@hotmail.com